Soft Matter

ARTICLE TYPE

Cite this: DOI: 00.0000/xxxxxxxxxx

Using Microprojectiles to Study the Ballistic Limit of Polymer Thin Films

Shawn H. Chen,[a*] Amanda J. Souna,[b] Christopher L. Soles,[b] Stephan J. Stranick,[a] and Edwin P. Chan[b*]

Received Date
Accepted Date

DOI: 00.0000/xxxxxxxxxx

The dynamic impact between a particle and a planar material is important in many high impact events, and there is a growing need to characterize the mechanical properties of light-weight polymeric materials at dynamic loading conditions. Here, a laser-induced projectile impact test (LIPIT) is employed to investigate the ballistic limit (V_0) and materials properties at impact velocities ranging from 40 m s^{-1} to 70 m s^{-1}. An analytical expression describing the various energy dissipation mechanisms is established to estimate the yield stress and elasticity for polycarbonate thin films. This measurement approach demonstrates the utility of using low sample mass for discovery of materials for impact mitigation, as well as high-throughput mechanical characterization at dynamic loading rates.

The collision of a particle with the surface of a solid body can result in several outcomes that can be either advantageous or detrimental depending on the particular materials application. The particle can bounce off the surface, become attached to the surface, or perforate the solid.[1–3] In additive manufacturing processes, it is desirable for microparticles to impinge onto the surface and consolidate into a solid form.[4] On the other hand, a projectile perforating a ballistic resistant coating or armor can be catastrophic if the desired outcome is impact mitigation.[5–7] Understanding the conditions that determine whether a particle attaches to or perforates a surface during dynamic impact is important in applications ranging from additive manufacturing to impact mitigation and ballistics protection.

A key parameter used to access a material's capacity to withstand a dynamic impact by a projectile without catastrophic failure is the ballistic limit (V_0).[8–10] V_0 represents the maximum projectile velocity that a material can withstand without perforation. Historically, V_0 has been difficult to measure accurately due to the statistical nature of ballistics testing. Ballistic testing of materials can also be time and resource intensive when statistically significant tests are properly carried out following testing guidelines. An alternative to the ballistic limit is V_{50}, which is the velocity when 50 % of the projectiles perforates the test object. It has been more widely adopted to characterize the performance and to estimate the ballistic limit of materials to circumvent some of the challenges associated with V_0 testing.[10]

A promising measurement platform that can potentially enable high-throughput mechanical characterization of impact mitigating materials at ballistic rates is the laser-induced projectile impact test (LIPIT).[11–14] LIPIT is a microparticle-based dynamic impact test that utilizes an ablation laser to accelerate a microprojectile towards a specimen at high velocities (10 m s^{-1} to 1000 m s^{-1}). The miniaturized geometry of LIPIT greatly reduces the large sample volume required for a typical ballistic test, which can be a challenge as procurement and synthesis of sufficient quantities of novel materials can be prohibitive. By scaling down the testing environment, the number of measurements can be scaled up for high-throughput testing of materials, overcoming some of the hurdles in traditional ballistics testing. However, the utilization of microparticles results in significantly lower momentum and kinetic energies compared to their macroscopic counterparts. It is unclear whether the dynamic impact phenomenon observed at the microscale correlates to the results on the macroscale. Previous results also revealed the difficulty in parsing out the ballistic limit of materials due to the limited control over the projectile velocity.[15,16] Nevertheless, these results help to inform the fracture behavior and intrinsic material properties at these dynamic loading rates, and could potentially provide additional insight on the effects of scale of the materials on impact mitigation.

Here, LIPIT is used to study the ballistic limit of polycarbonate (PC) thin films. PC is a highly relevant material for dynamic impact studies as it is a high-performance engineering plastic commonly used as lightweight transparent protection for applications in personal electronic devices, safety goggles, industrial machine guards, aircraft windscreens, and anti-ballistic armor.[9,17,18] PC's

[a] *Materials Measurement Sciences Division, National Institute of Standards and Technology, 100 Bureau Dr, Gaithersburg, MD 20899. Tel: +1 301-975-2140; E-mail: shawn.chen@nist.gov*

[b] *Materials Science and Engineering Division, National Institute of Standards and Technology, 100 Bureau Dr, Gaithersburg, MD 20899. Tel: +1 301-975-5228; E-mail: edwin.chan@nist.gov*

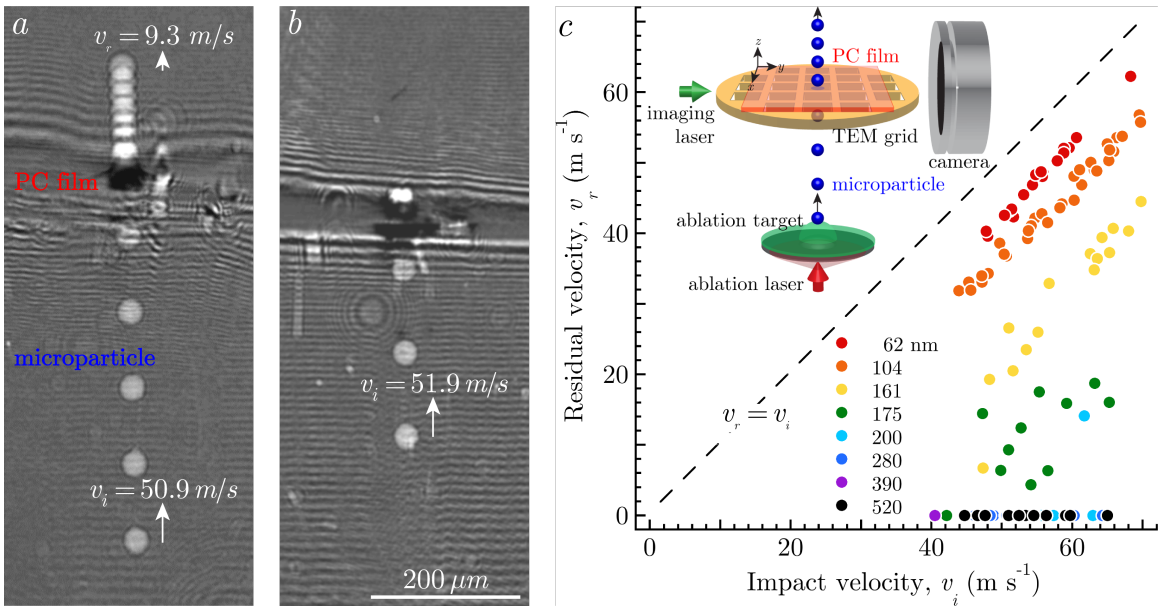

Fig. 1 The laser-induced projectile impact testing (LIPIT) of polycarbonate (PC) thin films. Representative stroboscopic images of the microparticle trajectory (impact velocities ≅ 51 m s^{-1}) for 174.9 nm ± 0.6 nm thick films (a) perforated by the microparticle and (b) resisted perforation. (c) Summary of the microparticle velocities before (v_i) and after (v_r) impacting PC thin films as a function of film thickness (h). The black line demarcates the upper limit of residual velocity (i.e. no energy transfer to the sample, $v_r = v_i$). The inset is the schematic of the LIPIT experiment. Error bars are within the size of the markers.

ductility is well known, which is attributed to the ability of the polymer chains to rearrange upon impact, which gives rise to the polymer's high toughness.[19–22] By conducting LIPIT experiments on PC films with a range of film thicknesses ($h \cong 60$ nm to 520 nm, error $\leq 1\%$) over a narrow range of impact velocities, we experimentally quantify the critical thickness at the ballistic limit of these nanoscale films.

Stroboscopic illumination captures the trajectory of the microprojectile before and after the impact event on a single image (**Figures 1a and 1b**). From this image, the particle velocity ($v = \Delta\delta/\Delta t$) can be calculated by measuring the spacing of the microparticle positions ($\Delta\delta$) with Δt fixed by the frequency of the strobe. Velocities between 40 m s^{-1} to 70 m s^{-1} were used to probe the intermediate rates of deformation of the PC films. **Figure 1c** plots the residual velocity (v_r) of the projectiles as a function of the impact velocity (v_i) for all of the PC films investigated. The dashed line indicates the case in which there is no velocity change ($v_r = v_i$). Using these results, we can quantify the energy absorption of the PC films as a function of film thickness and microprojectile velocities. Assuming the impact event is an inelastic collision between the projectile and a plug of the film, the energy transfer within the system can be represented as:[23]

$$\frac{1}{2}m_p v_i^2 = \frac{1}{2}(m_p + m_f)v_r^2 + E_d \quad (1)$$

where m_p is the mass of the projectile with a diameter of $2a_p$ and m_f is the mass of a plug of the film that interacts with the projectile with a given film thickness (h). We note that m_f is an "effective" mass related to a_f, which can be regarded as an effective plug radius of the film that is dependent on v_i. Both parameters depend on the dimension of the film that interacts with the projectile of a given mass (m_p), as well as the material properties of the film. The left side of **Equation 1** is the initial kinetic energy of the projectile. On the right side, the first term represents the kinetic energy of the projectile and the plug after collision. The second term, E_d, encompasses the various dissipation mechanisms through which the kinetic energy of the projectile is lost, such as air drag, generation of sound, heat, film deformation, and crack formation. At $v_i = 55$ m s^{-1}, approximately half of the microprojectiles successfully perforate 175 nm thick samples. This is analogous to the V_{50} values reported in literature on traditional ballistics testing, and can be a useful metric to compare the LIPIT results against existing ballistic measurements.

The geometric form of most impact mitigation materials is a planar slab or sheet. Therefore, an important design criteria in the materials' impact response is the sample thickness as it directly correlates to its inertial deformation resistance. At the impact velocities measured in this work, PC thin films were observed to have a similar failure mechanism as those of metallic plates impacted with spherical projectiles.[9,24] When film thickness is low, plugging and ductile yielding occur upon projectile impact. Radial cracks initiate and propagate at the edge of the impacting projectile and lead to plugging of the film(**Figure 2**). The region further from the plug undergoes plastic yielding as the material flows around the periphery of the projectile.

The ductile yielding characteristic of PC causes film thickness and refractive to change.[25] As a result, the deformation regions appear darker. As shown in **Figure 2a,b**, the post-impact phase-contrast and dark-field micrographs of the 100 nm thick PC film highlight the significant yielding that occur in the region of impact, with damage extending out further than the diameter of the projectile. Within the damage zone, petal-like features extending

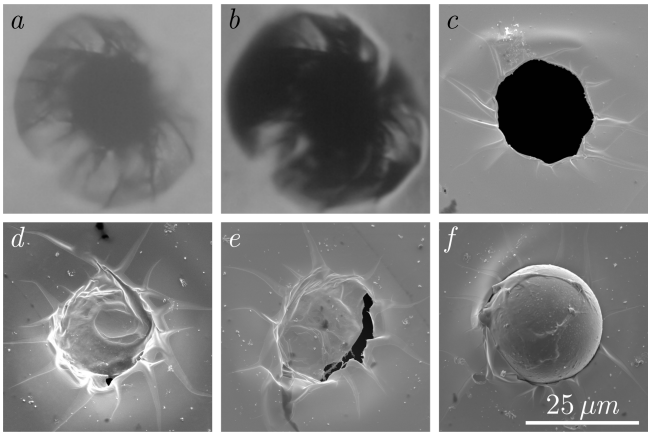

Fig. 2 (a) Phase-contrast and (b) dark-field optical images of a perforated site highlighting the highly deformed region for a 100 nm PC film. (c) SEM micrograph from the top surface of the same region (particle travelling out-of-the-page). (d-f) Doming and partial perforation of a 175 nm sample from a projectile impact. Scalebar for all the images =25 μm.

out from the central impact region in a radial direction is observed, reminiscence of the fractures previously observed in brittle material such as polystyrene and graphene oxide films.[11,26] Upon further inspection of the surface with an scanning electron microscope (SEM), it becomes clear that the features are instead wrinkles and folds formed by the plastically stretched films (**Figure 2c**). The plastically stretched regions of the film, known as shear deformation zones (DZs), is characteristic of PC that can undergo mixed mode deformation.[20,25] At high film thicknesses, a projectile lacks the momentum to perforate the film, but still causes DZs to form (**Figure 2d,e**).[9] Literature on ballistic impact of metallic plates describes catastrophic shear plugging as the interplay between thermal softening (from adiabatic heating) and work hardening (from yielding) of the material within a band of highly sheared material is produced at a radial position close to the projectile radius.[27–29] While it is difficult to assess the contributions of thermal instability to fracture that results in plugging from the current experiments, it is evident from the melted polymer that wraps around the captured projectile in **Figure 2f** that local adiabatic heating does occur and cannot be ignored. While failure in the form of petalling was not observed in our PC films, ductile yielding and plugging occurs.

Intuitively, a thinner film is less effective at slowing down a projectile compared to a thicker one. There is less mass to absorb or dissipate the energy of impact, and the interaction time between the sample and the projectile is shorter resulting in stress localization near the impact site.[30,31] We can express this change in mass of the film, and the resultant change in the total kinetic energy of the system due to this inelastic collision event (**Figure 3a**) by rearranging **Equation 1**,

$$\begin{aligned} v_r^2 &= \frac{m_p}{(m_p+m_f)} v_i^2 - \frac{2E_d}{(m_p+m_f)} \\ &= \alpha {v_i}^2 - \gamma \end{aligned} \tag{2}$$

The parameters, $\alpha = \frac{m_p}{m_p+m_f}$ is the ratio of the projectile mass relative to the total mass of the system following impact, and $\gamma = \frac{2E_d}{m_p+m_f}$ is the energy dissipation term normalized by the total mass. The square of the incident and residual velocities across different film thicknesses are related by the coefficient α, which is determined from the results in **Figure 3b**. The coefficient α is the fraction of initial kinetic energy that is conserved (see Supporting Information). Representing the results this way enables the separation of the mass dependence of the system from the analysis. The y-intercept (γ) yields the "specific" energy dissipation of the film at the ballistic limit.

At the moment of impact, the projectile sends a stress wave into the material.[32,33] At low impact velocities, the stress wave can alter the effective bending stiffness of the sample and change the location where failure initiates, leading to spalling or fragmentation of the back-surface.[30,34] To cause a plug of material to develop and become displaced, work must be done to cause fracture. In this geometry, the work of fracture (W_f) is related to the film thickness as,

$$W_f \cong \pi a_f \sigma_Y h^2 \tag{3}$$

where σ_Y is the yield stress of the film and a_f is the radius of the plug material. It's important to note that $a_f \geq a_p$ since its size should be determined by the location of the fracture initiation sites and is therefore dependent on v_i. The bending of the film by the impact of the microparticle can be represented as the elastic bending energy:[31,35]

$$E_{el} \cong \frac{1}{2} \frac{E_f^* h^3}{c_\delta l^2} {\delta_f}^2 \tag{4}$$

where $E_f^* = E_f/(1-{\nu_f}^2)$ is plane-strain elastic modulus, ν_f is the Poisson's ratio of the film, l is the lateral dimension of the film undergoing deflection, and δ_f is the out-of-plane deformation of the film. The geometric constant, c_δ, is related to the deformation profile of the film due to the impacting microparticle and is a function of ν_f, l, and δ_f.[36] The observed energy loss (E_d) is the sum contribution of the air drag of the microparticle (E_{drag}), thermal work of the impact event (W_T),[37] work of fracture (W_f), and elastic bending energy (E_{el}),[38]

$$E_d = E_{drag} + W_T + W_f + E_{el} \tag{5}$$

As the film thickness increases, the energy required to move a plug of material increases until the maximum energy available from the projectile for a given velocity is reached. At this point the remaining energy is insufficient to cause perforation. Deceleration of the microprojectiles due to air drag is found to be negligible with the materials and testing conditions used in this study. Specifically, we estimate that the contributions of air drag due to the film displacing the surrounding air ($\approx E_{drag}/(m_p v_i^2/2) = C_d \rho_{air} \pi a_f^2 \delta_f / m_p$) to be ≈ 1.4 % of the initial kinetic energy thus $E_{drag} \cong 0$. It is evident from **Figure 2** that there is melting and thermal softening around the region of impact. Therefore, energy dissipation through thermal processes at these dynamic impact rates cannot be neglected. Since adiabatic work is related to

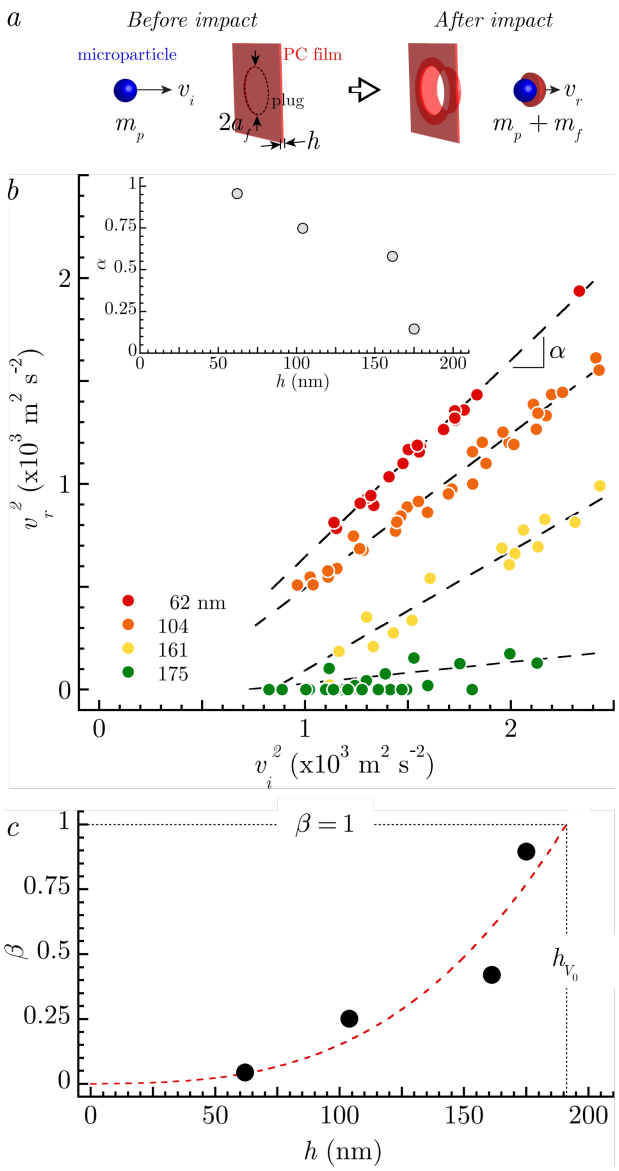

Fig. 3 (a) Schematic representation of an inelastic collision between a microparticle and a plug of material removed from the PC film. (b) Plot of v_r^2 vs. v_i^2. The slope of each data set is α for the particular film thickness (h) for films when perforation occurred. The inset is a plot of α vs. h. (c) Fraction of kinetic energy loss ($\beta = 1 - \alpha$) vs. h. The fit corresponds to Equation 7. Extrapolating to $\beta = 1$ yields h_{V_0}, which is the critical thickness at the ballistic limit (V_0).

the applied pressure of the microprojectile imposed onto the film that scales with v_i ($\approx \rho_p {v_i}^2$), we approximate the thermal work as,

$$W_T \cong \rho_p {v_i}^2 V_f \tag{6}$$

where ρ_p is the density of the microparticle and $V_f \cong \pi {a_f}^2 h$ is the volume of the film.

The fraction of the kinetic energy loss ($\beta = 1 - \alpha$) during an inelastic collision is defined as the ratio of the dissipation energy and the initial kinetic energy (details of the derivation are provided in the Supporting Information). Substituting **Equation 3**, **Equation 4** and **Equation 6** into **Equation 5** yields,

$$\beta = \frac{E_d}{\frac{1}{2} m_p {v_i}^2} = D_0 + D_1 h + D_2 h^2 + D_3 h^3 \tag{7}$$

where D_0 is the drag term, $D_1 \cong \frac{{a_f}^2}{{a_p}^3}$ is the term associated with thermal work, $D_2 = \frac{2\pi a_f \sigma_Y}{m_p {v_i}^2}$ and $D_3 = \frac{E_f^* (\delta_f / l)^2}{c_\delta m_p {v_i}^2}$.

The plot of β vs. h (**Figure 3c**) gives insight into the effects of film geometry on microballistic perforation resistance for polymer thin films. At low film thickness, most of the initial kinetic energy is conserved after impact and $\beta << 1$. With increasing film thickness, β increases and the contribution of elastic bending to β becomes more dominant ($\sim h^3$) compared to yielding ($\sim h^2$). The available kinetic energy is increasingly lost through elastic bending until it becomes the primary dissipative mechanism, and the remaining kinetic energy of the microparticle is insufficient to perforate the film. At an average impact velocity of $v_i = 55$ m s^{-1}, **Equation 7** predicts that the critical film thickness (h_{V_0}) is approximately 190 nm when $\beta = 1$. In other words, $V_0 = 55$ m s^{-1} for a 190 nm thick PC film. This prediction is experimentally confirmed by the LIPIT results (**Figure 1c**), whereby PC films with $h \geq 200$ nm successfully stop microprojectiles with $v_i \leq 55$ m s^{-1}.

In addition to determining V_0, we apply **Equation 7** to fit the results in **Figure 3c** to obtain $D_1 \cong 1 \times 10^{-4}$ nm^{-1}, $D_2 \cong 1.2 \times 10^{-7}$ nm^{-2} and $D_3 \cong 1.39 \times 10^{-7}$ nm^{-3} by substituting $v_i = V_0 = 55$ m s^{-1}. The magnitude of D_1 would suggest that the fraction of initial kinetic energy dissipated in the form of thermal work for a PC with $h = 200$ nm at the ballistic limit is approximately 2 %. It is difficult to assess the contribution of thermal work without additional measurements to confirm the thermal property changes of our materials. However, previous result[39] on the high rate compression testing for PC show that adiabatic heating does not appear to contribute significantly, which is consistent with our results suggesting that the primary mechanisms of energy dissipation is associated with yielding and bending. Based on the expressions for D_2 and D_3, we estimate $\sigma_Y \cong 95$ MPa and $E_f^* \cong 6.4$ GPa, respectively. The estimated yield stress is comparable with the Kolsky bar testing reported from Sarva and Boyce by extrapolating their model to the strain rates presented in this work ($\approx 10^5$ s^{-1})[17] and assuming $a_f \cong a_p = 12.5$ μm. The estimated value for E_f^*, determined based on deflection of a plate by a concentrated load (i.e. impact by the microparticle), with $c_\delta \approx 0.0008$ and $\delta_f / l \approx 1$,[36] is also comparable to reported literature values at the highest strain rate studied ($\approx 10^3$ s^{-1}) for bulk PC samples. A direct comparison of E_f^* at comparable strain rates

is not possible at this time, but efforts to modify LIPIT are currently underway to directly measure the elasticity of PC thin films at these dynamic deformation rates.

This work demonstrates the application of LIPIT as a measurement approach for characterizing the ballistic limit of PC thin films. The results show that both the observed failure mechanism and the measured impact resistance depend strongly on specimen geometry and the rate of deformation. Specifically, decreasing the film thickness and/or increasing the impact velocity can greatly reduce the impact resistance of the material. Our treatment of the experimental results enables the prediction and determination of a material's ballistic limit as a function of film thickness. While the work of fracture and plastic yielding may appear to be the primary modes of energy dissipation, contribution of the film's elastic bending stiffness and local adiabatic heating cannot be overlooked. The small sample mass requirement and high-throughput nature of the technique further highlights LIPIT as a viable high-rate impact test for materials discovery. Testing over a wider range of deformation rates, which is an ongoing effort for LIPIT, can aid in bridging the measurement gap between traditional quasi-static punch tests and ballistic tests.

Conflicts of interest

Certain instruments and materials are identified in this paper to adequately specify the experimental details. Such identification does not imply recommendation by the National Institute of Standards and Technology; nor does it imply that the materials are necessarily the best available for the purpose.

Acknowledgements

SHC acknowledges financial support from the NIST National Research Council Postdoctoral Research Associateship. This work is a contribution of NIST, an agency of the U.S. Government, and not subject to U.S. copyright.

Notes and references

1 I. M. Hutchings and R. E. Winter, *Wear*, 1974, **27**, 121–128.

2 I. M. Hutchings, R. E. Winter and J. E. Field, *Proceedings of the Royal Society of London. A. Mathematical and Physical Sciences*, 1976, **348**, 379–392.

3 W. Johnson, A. K. Sengupta and S. K. Ghosh, *International Journal of Mechanical Sciences*, 1982, **24**, 425–436.

4 S. V. Klinkov, V. F. Kosarev and M. Rein, *Aerospace Science and Technology*, 2005, **9**, 582–591.

5 M. E. Backman and W. Goldsmith, *International Journal of Engineering Science*, 1978, **16**, 1–99.

6 P. V. Cavallaro, *Soft Body Armor: An Overview of Materials, Manufacturing, Testing, and Ballistic Impact Dynamics*, Naval Undersea Warfare Center Technical Report NUWC-NPT-TR-12-057, 2011.

7 R. A. Bizao, L. D. Machado, J. M. d. Sousa, N. M. Pugno and D. S. Galvao, *Scientific Reports*, 2018, **8**, 1–8.

8 R. L. Woodward, S. R. Tracey and I. G. Crouch, *Journal de Physique IV*, 1991, **1**, 277–282.

9 S. C. Wright, N. A. Fleck and W. J. Stronge, *International Journal of Impact Engineering*, 1993, **13**, 1–20.

10 T. H. Johnson, L. Freeman, J. Hester and J. L. Bell, *IEEE Access*, 2014, **2**, 1442–1455.

11 J.-H. Lee, P. E. Loya, J. Lou and E. L. Thomas, *Science*, 2014, **346**, 1092–1096.

12 D. Veysset, A. J. Hsieh, S. Kooi, A. A. Maznev, K. A. Masser and K. A. Nelson, *Scientific Reports*, 2016, **6**, 1–6.

13 J. Hyon, O. Lawal, O. Fried, R. Thevamaran, S. Yazdi, M. Zhou, D. Veysset, S. E. Kooi, Y. Jiao, M.-S. Hsiao, J. Streit, R. A. Vaia and E. L. Thomas, *Materials Today*, 2018, **21**, 817–824.

14 E. P. Chan, W. Xie, S. V. Orski, J.-H. Lee and C. L. Soles, *ACS Macro Letters*, 2019, **8**, 806–811.

15 J.-H. Lee, D. Veysset, J. P. Singer, M. Retsch, G. Saini, T. Pezeril, K. A. Nelson and E. L. Thomas, *Nature Communications*, 2012, **3**, 1–9.

16 D. Veysset, S. E. Kooi, A. A. Maznev, S. Tang, A. S. Mijailovic, Y. J. Yang, K. Geiser, K. J. Van Vliet, B. D. Olsen and K. A. Nelson, *Journal of the Mechanical Behavior of Biomedical Materials*, 2018, **86**, 71–76.

17 S. Sarva and M. Boyce, *Journal of Mechanics of Materials and Structures*, 2007, **2**, 1853–1880.

18 A. Dorogoy, D. Rittel and A. Brill, *International Journal of Impact Engineering*, 2011, **38**, 804–814.

19 A. M. Donald and E. J. Kramer, *Journal of Materials Science*, 1981, **16**, 2967–2976.

20 A. M. Donald and E. J. Kramer, *Journal of Materials Science*, 1981, **16**, 2977–2987.

21 J. Y. Jho and A. F. Yee, *Macromolecules*, 1991, **24**, 1905–1913.

22 C. Xiao, J. Y. Jho and A. F. Yee, *Macromolecules*, 1994, **27**, 2761–2768.

23 R. Cross, *Sports Engineering*, 2014, **17**, 3–22.

24 G. G. Corbett, S. R. Reid and W. Johnson, *International Journal of Impact Engineering*, 1996, **18**, 141–230.

25 R. P. Kambour, *Polymer*, 1964, **5**, 143–155.

26 W. Xie, A. Alizadeh-Dehkharghani, Q. Chen, V. K. Champagne, X. Wang, A. T. Nardi, S. Kooi, S. Müftü and J.-H. Lee, *Scientific Reports*, 2017, **7**, 1–9.

27 T. A. C. Stock and K. R. L. Thompson, *Metallurgical Transactions*, 1970, **1**, 219–224.

28 R. L. Woodward, *International Journal of Mechanical Sciences*, 1978, **20**, 599–607.

29 R. F. Recht, *Journal of Applied Mechanics*, 1964, **31**, 189–193.

30 R. Olsson, M. V. Donadon and B. G. Falzon, *International Journal of Solids and Structures*, 2006, **43**, 3124–3141.

31 D. P. Holmes and A. J. Crosby, *Physical Review Letters*, 2010, **105**, 038303.

32 R. Olsson, *Composites Part A: Applied Science and Manufacturing*, 2000, **31**, 879–887.

33 R. Olsson, *Composites Part A: Applied Science and Manufacturing*, 2001, **32**, 1207–1215.

34 H. J. Prentice, W. G. Proud, S. M. Walley and J. E. Field, *International Journal of Impact Engineering*, 2011, **38**, 849–863.

35 H. Singh and P. Mahajan, *Composite Structures*, 2016, **149**, 79–92.
36 J. C. Heap, *Journal of Engineering for Industry*, 1968, **90**, 268–278.
37 D. Rittel, *Mechanics of Materials*, 1999, **31**, 131–139.
38 K. N. Shivakumar, W. Elber and W. Illg, *Journal of Applied Mechanics*, 1985, **52**, 674–680.
39 M. J. Kendall and C. R. Siviour, *Philosophical Transactions of the Royal Society A*, 2014, **372**, 20130202.